In Vitro and In Vivo Enzyme-Mediated Biomineralization of Oligo(poly(ethylene glycol) Fumarate Hydrogels

Matilde Bongio, M. Reza Nejadnik, Z. Tahmasebi Birgani, Pamela Habibovic, Lucas A. Kinard, F. Kurtis Kasper, Antonios G. Mikos, John A. Jansen, Sander C. G. Leeuwenburgh, Jeroen J. J. P. van den Beucken*

The enzyme alkaline phosphatase (ALP) is added at different concentrations (i.e., 0, 2.5, and 10 mg · ml^{-1}) to oligo(poly(ethylene glycol)fumarate) (OPF) hydrogels. The scaffolds are either incubated in 10 mM calcium glycerophosphate (Ca–GP) solution for 2 weeks or implanted in a rat subcutaneous model for 4 weeks. Fourier transform infrared (FTIR) spectroscopy, X-ray diffraction (XRD), scanning electron microscopy (SEM), energy dispersive spectroscopy (EDS), and alizarin red staining show a strong ability to form minerals exclusively in ALP-containing hydrogels in vitro. Additionally, the calcium content increases with increasing ALP concentration. Similarly, only ALP-containing hydrogels induce mineralization in vivo. Specifically, small (≈5–20 μm) mineral deposits are observed at the periphery of the hydrogels near the dermis/scaffold interface using Von Kossa and alizarin red staining.

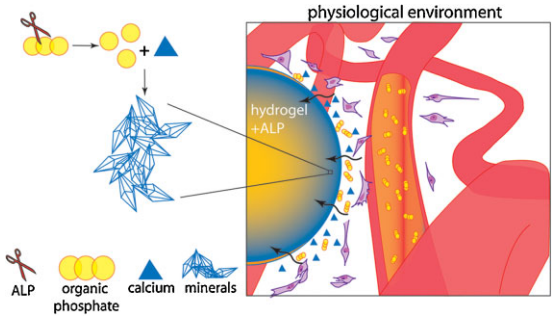

M. Bongio, Dr. M. Reza Nejadnik, Prof. J. A. Jansen, Dr. S. C. G. Leeuwenburgh, Dr. J. J. J. P. van den Beucken
Department of Biomaterials, Radboud University Nijmegen Medical Centre, P.O. Box 9101, 6500 HB Nijmegen, The Netherlands
E-mail: j.vandenbeucken@dent.umcn.nl
Z. Tahmasebi Birgani, Dr. P. Habibovic
Department of Tissue Regeneration, University of Twente, MIRA Institute for Biomedical Technology and Technical Medicine, P.O. Box 217, 7500-AE, Enschede, The Netherlands
L. A. Kinard, Prof. A. G. Mikos
Department of Chemical and Biomolecular Engineering, Rice University, P.O. Box 1892, Houston, TX 77251-1892, USA
Dr. F. Kurtis Kasper, Prof. A. G. Mikos
Department of Bioengineering, Rice University, P.O. Box 1892, Houston, TX 77251-1892, USA

M. Bongio and M. R. Nejadnik contributed equally to this work.

1. Introduction

Bone is a type of connective tissue with a hierarchical organized structure made of collagen fibrils (≈35% of dry weight) reinforced with nano-hydroxyapatite minerals (≈65% of dry weight).[1] This combination of organic and inorganic phases confers unique biological functions (e.g., mineralization) and mechanical properties (e.g., elasticity, resilience, and strength) to native bone.[2] Over the past few years, the design and development of substitutes mimicking the structure and biological performances of bone has gained increasing interest. Ceramic-based or polymer-based bone substitutes in the form of malleable and degradable pastes, putties or viscous solutions are principally employed for non-load bearing applications; for example, as bone-void fillers or augmentation materials in areas requiring trabecular bone rather than cortical bone.[3]

In the context of polymer-based bone substitutes, hydrogels are particularly promising material candidates. Hydrogels are three-dimensional networks of polymer chains that are highly hydrated and present mechanical behavior and viscoelastic structures similar to the extracellular matrix of soft tissues. More importantly, their composition and microarchitecture determine a favorable milieu for the survival and delivery of cells and/or drugs into the harsh environment of the damaged tissue.[4] Initially, hydrogels were predominantly investigated as materials for soft tissue applications. Over the past decade, the beneficial properties of these materials, including chemical tunability, ease of functionalization, controllable degradation, and biological relevance, has encouraged researchers to broaden the use of hydrogels also for hard tissue applications. Nevertheless, mechanical weakness and poor mineralization, which prevent the formation of a strong chemical bond between hydrogel and adjacent bone tissue (i.e., low bone-hydrogel interfacial adhesion strength), are the major drawbacks for bone regenerative applications.[5]

In order to render these materials suitable for applications in bone tissue regeneration, researchers have developed strategies focused on inducing mineralization in inert, non-mineralized hydrogels.[6] Briefly, these mineralization approaches can be categorized into three main groups: i) incorporation of bioactive inorganic phases, including calcium phosphate[7–9] and bioglasses;[10] ii) use of biological elements involved in the biomineralization process, including saturated solutions of calcium (Ca^{2+}) and phosphates (PO_4^{3-}),[11,12] enzymes,[13,14] or synthetic analogs to matrix vesicles[15] that play a fundamental role on the nucleation and growth of hydroxyapatite; and iii) functionalization of the hydrogel backbone with anionic ligands that attract calcium ions.[16,17] Unlike the first and third approaches, which may require complex chemical procedures, the incorporation of biological elements is simple and applicable to many types of hydrogel-based systems.

In the current study, an enzymatic approach was followed via the incorporation of alkaline phosphatase (ALP) into a synthetic PEG-based hydrogel (i.e., oligo(poly(ethylene glycol) fumarate) (OPF)). In nature, ALP is a glycolipid-anchored membrane protein of cells and matrix vesicles involved in the early stages of biomineralization of hard tissue.[18] Although the mechanism of action has not been fully elucidated, the leading theory, first elaborated by Robison in 1923, is that the enzyme hydrolyses organic phosphate-monoesters to increase the concentration of inorganic phosphate, thereby causing local supersaturation and nucleation of inorganic crystals.[19] The enzyme ALP for biomineralization has been used previously to prepare hydrogel composites, such as collagen,[20] alginate,[21] and peptide amphiphile (PA) gels.[22] Our laboratory has recently demonstrated the feasibility of inducing formation of CaP minerals within different hydrogels by incorporating ALP during the polymerization process without the need for immobilization by chemical binding.[14] The same work also proved that ALP remains entrapped within the cross-linked polymeric network due to its relatively high molecular weight (approximately 185 kDa).[23]

OPF, a PEG-based oligomer featuring fumarate ester groups, has been developed for tissue engineering applications in the form of a biodegradable injectable hydrogels and has shown minimal cytocompatibility in vitro[7,24] and excellent biocompatibility in vivo.[25,26] On the other hand, OPF hydrogels alone are bioinert to cells and proteins (e.g., growth factors), that have an essential role in modulating attachment, proliferation, and differentiation of osteoblasts.[9] Therefore, the incorporation of ALP into OPF hydrogels was considered to be a valid strategy to induce the formation of apatite crystals, which exhibit high affinity for proteins, and enhance the bioactivity and mineralization capacity of the final constructs to be used in bone tissue engineering.

The aim of the present study was to compare the in vitro and in vivo efficacy of ALP to induce biomineralization in OPF hydrogels using a calcium glycerophosphate solution as substrate for in vitro experiments and subcutaneous implantation model in rats, respectively. In order to investigate the effect of enzyme concentration on mineral formation, different amounts of ALP were added to OPF hydrogel precursor solutions. We hypothesized that: i) it is possible to induce biomineralization within OPF hydrogels in vitro and in vivo, and ii) the extent of biomineralization is proportional to the amount of incorporated ALP.

2. Experimental Section

2.1. Reagents

Fumaryl chloride was obtained from Acros (Pittsburgh, PA, USA). Poly(ethylene glycol) (PEG) was purchased from Aldrich (Milwaukee, WI, USA). Poly(ethylene glycol) diacrylate (PEGDA) (nominal molecular weight 3400 Da) was obtained from Glycosan Biosystem (Salt Lake City UT, USA). *N*,*N*,*N*′,*N*′-tetramethylethylenediamine (TEMED) was purchased from Fluka (Buchs, Switzerland). Ammonium persulfate (APS), phosphate-buffered saline pH 7.4 (PBS), enzyme ALP (EC3.1.3.1, bovine intestinal mucosa, 7 500 units $\cdot$ mg^{-1}) and glycerophosphate calcium salt (molecular weight 210.14 g $\cdot$ mol^{-1}) were purchased from Sigma–Aldrich (St. Louis MO, USA).

2.2. OPF Synthesis

PEG of nominal number-average molecular weight of 10 000 g $\cdot$ mol^{-1} and fumaryl chloride were used to synthesize OPF, as

Macromolecular Journals

Macromol. Biosci. **2013**, DOI: 10.1002/mabi.201200474

described by Kinard.[27] The purified macromer was stored at –20 °C.

2.3. Hydrogel Scaffold Preparation

OPF hydrogels with three different concentrations of ALP (i.e., 0 mg · ml^{-1} (OPF), 2.5 mg · ml^{-1} (OPF-low ALP) and 10 mg · ml^{-1} (OPF-high ALP)), were prepared as outlined in Table 1. OPF and PEGDA were sterilized by exposure to UV light (wavelength 366 nm, CAMAG UV Lamp, SelectScience, Bath, United Kingdom) for 3 h and freeze-dried overnight following an established method.[23] MilliQ H_2O, ALP solutions (12.5 mg · ml^{-1} in MilliQ H_2O), APS (0.3 M) and TEMED (0.3 M) were filter sterilized using a 0.2 μm filter. For OPF preparation, 0.15 g of OPF and 0.075 g of PEGDA were added to 860 μl of MilliQ H_2O. For OPF-low ALP and OPF-high ALP formulations, equal amounts of OPF and PEGDA were added to 660 μl of MilliQ H_2O and 200 μl of ALP solution (OPF-low ALP) and 60 μl of MilliQ H_2O and 800 μl of ALP solution (OPF-high ALP), respectively, in order to obtain the aforementioned concentrations. The formulations were shaken at room temperature for 30 min to obtain complete dissolution of the polymers. Equal volumes (70 μl) of redox initiators, APS and TEMED, were then added and gently mixed. A volume of 200 μl of the polymer mixtures was injected into wells of a 96-well plate and incubated for 30 min at 37 °C. After gel formation, the hydrogels were transferred to 12-well plates. 4 ml of MilliQ H_2O was added and changed after 1 h and 1 d to ensure the removal of unreacted products.

2.4. Analysis of ALP Distribution within the Hydrogels

A protein-specific dye, Coomassie brilliant blue R-250 (0.1% w/v in MilliQ H_2O, Merck, Darmstadt, Germany) was used to visualize the spatial distribution of ALP within OPF hydrogels. Specifically, the dye was used to stain both whole scaffolds and 50 μm-thick cryosections for 1 h at room temperature. Afterwards, samples were washed three times in MilliQ H_2O. Microscopic images were taken using an optical microscope (Axio Imager Microscope Z1, Carl Zeiss Micro imaging GmbH, Göttingen, Germany).

2.5. Analysis of Diffusion in Hydrogels

In order to study the diffusion of compounds into the ALP-containing hydrogels, samples were incubated in a tetramethylrhodamine (TRITC)-dextran solution (12.5 μg · ml^{-1} in MilliQ H_2O; MW 10 000 Da, Alexa Fluor 568, Molecular Probes, Eugene, Oregon, USA) for 1 d at 37 °C, and washed in MilliQ H_2O. Microscopic images were taken using an Olympus FV1000 confocal laser scanning microscope (CLSM) with a 40× water immersion objective (Olympus, Center Valley, PA, USA).

2.6. In Vitro Experiments

2.6.1. Incubation of Hydrogels

In order to study the deposition of minerals, hydrogels were incubated in MilliQ H_2O supplemented with 10 mM calcium glycerophosphate (Ca–GP, pH = 9.55 ± 0.05) for 2 weeks at 37 °C followed by refreshing the medium twice a week. Afterwards, hydrogels were washed two times for 2 h with MilliQ H_2O and incubated 1 d in MilliQ H_2O to ensure complete removal of Ca–GP residues

2.6.2. Hydrogel Swelling Experiment

Swelling ratio of hydrogels swollen in MilliQ H_2O overnight (before soaking) and in 10 mM Ca-GP for 2 weeks (after soaking), were calculated by the Equation 1:

$$(W_s - W_d)/W_d \quad (1)$$

in which W_s and W_d are the weight of the hydrogels in swollen and freeze-dried states, respectively. The swelling ratio is defined as the fractional increase in the weight of the hydrogel due to water absorption.[28] A total of $n = 3$ replicates per time point for each experimental conditions were used.

2.6.3. Characterization of Biomineralization

Biomineralization within the OPF-based hydrogels was characterized using a range of analytical techniques, including attenuated total reflection Fourier transform infrared spectroscopy (ATR-FTIR) (Perkin–Elmer, Spectrum One, Groningen, The Netherlands), X-ray diffraction (XRD) (Philips, PW 1830, Almelo, The Netherlands), and the orthocresolphtalein complexone (OCPC) method (Sigma–Aldrich Chemie BV, Zwijndrecht, The Netherlands).

Hydrogels were freeze-dried for 48 h before the analyses. Specifically, ATR-FTIR and XRD with Cu K_α-radiation (wavelength 1.54056 Å, voltage 40 kV, current 30 mA) were used to characterize the chemical composition and crystallographic structures of the minerals within the hydrogels.

Table 1. Compounds and relative amounts used to prepare 1 ml of OPF-based hydrogels.

	ALP [mg · ml^{-1}]	OPF [g]	PEGDA [g]	MilliQ H_2O [μl]	ALP (12.5 mg · ml^{-1}) [μl]	APS 0.3 M [μl]	TEMED 0.3 M [μl]
OPF	0	0.15	0.075	860	–	70	70
OPF-low ALP	2.5	0.15	0.075	660	200	70	70
OPF-high ALP	10	0.15	0.075	60	800	70	70

The OCPC method was performed to measure the amount of calcium deposition within the hydrogels. Briefly, 1 ml of 0.5 N acetic acid was added to the freeze-dried hydrogels and placed on a shaker table overnight to dissolve mineral deposits. A volume of 10 μl samples or standards were incubated with 300 μl of working solution in a 96-well plate. The standards (range: 0–100 $\mu g \cdot ml^{-1}$) were prepared using a $CaCl_2$ stock solution. The absorbance of each well was measured on a microplate spectrophotometer at 570 nm. Data were obtained from triplicate samples and measured in duplicate.

2.6.4. Structure and Distribution of Minerals

The distribution of mineral within OPF-based hydrogels was visualized by means of field emission scanning electron microscopy (FESEM) (Jeol 6330, Tokyo, Japan), energy dispersive spectroscopy (EDS) (EDAX, AMETEK Materials Analysis Division, Mahwah NJ, USA), and microscopic analysis.

FESEM was performed on freeze-dried scaffolds, coated with a thin gold layer, to observe the morphology of the external and internal surface of the scaffolds. In order to examine the internal microstructure, the hydrogels were cut in half with a scalpel.

In order to preserve the shape and quality of mineralized hydrogels for EDS studies, samples were fixed in 10% neutral buffered formalin solution for 2 d, dehydrated in a graded series of alcohol (70–100%) and embedded in methylmethacrylate (MMA). After polymerization in MMA, transversel microtome sections (50–100 μm) were prepared using a microtome with a diamond blade (Leica Microsystems SP 1600, Nussloch, Germany). EDS was carried out at a low magnification and an accelerating voltage of 10 kV in a line scan mode on gold sputtered sections to improve the conductivity of the samples. Specifically, a line was drawn over a random diagonal of the disk-shaped samples and the counts of Ca and P were measured over the line (one reading every 0.1 μm). This measurement was repeated three times. The obtained values for Ca and P in each 10 μm-long section of the line were averaged and reported as the relative amount of the elements in that area.

Thinner MMA sections (6 μm) were prepared using a microtome with a diamond blade for staining with alizarin red to visualize calcium deposits. Microscopic images were taken using an optical microscope (Axio Imager Microscope Z1, Carl Zeiss Micro imaging GmbH, Göttingen, Germany).

2.7. In Vivo Experiment

2.7.1. Surgical Procedure

In order to analyze the biomineralization capacity under in vivo conditions, OPF-based hydrogels were implanted subcutaneously in eighteen skeletally mature male Wistar rats (250 g). The study was reviewed and approved by the Experimental Animal Committee of the Radboud University Nijmegen, The Netherlands (DEC 2011-023), and national guidelines for the use and care of laboratory animals were obeyed. Surgery was performed under general inhalation anesthesia by a mixture of isoflurane/N_2O/O_2 (Rhodia Organique Fine Limited, Avonmouth, Bristol, United Kingdom). Analgesic treatment was performed with subcutaneous injections of buprenorfine (0.02 $mg \cdot kg^{-1}$ body weight, Temgesic; Reckitt Benckiser Health Care Limited, Schering-Plough, United Kingdom) directly preoperatively and two times a day for 2 d postoperatively. The dorsum of the animal was shaved and disinfected with povidone iodine. Two paravertebral incisions of about 10 mm were made through the full thickness of the skin, one on each side of the vertebral column. Subcutaneous pockets were created by blunt dissection on the lateral side of the incisions. One hydrogel was inserted deep into each pocket and the skin was closed with resorbable sutures. In total, 36 scaffolds were implanted ($n = 12$ for each experimental group). The animals were housed in pairs in a filter top cage and given water and chow ad libitum. Further, the animals were daily examined with focus on body weight, dehydratation, infections, and proper activity. At 4 weeks post-implantation, all rats were euthanized by CO_2/O_2-asphyxiation.

2.7.2. Sample Retrieval and Histological Analysis

Immediately after euthanasia, subcutaneous scaffolds with surrounding tissue were retrieved and fixed in 10% neutral buffered formalin solution for 2 d. Subsequently, the tissue blocks were dehydrated through graded series of ethanol (70–100%), cut in half and embedded in paraffin. Using a microtome (Leica RM 2165, Leica Microsystems, Nussloch, Germany), six sections (6 μm) of each specimen were prepared and stained with hematoxylin–eosin (HE) for general histological examination of tissue responses, and with Von Kossa and alizarin red to detect phosphates and calcium deposits, respectively. Digital images were taken using an optical microscope (Axio Imager Microscope Z1, Carl Zeiss Micro imaging GmbH, Göttingen, Germany).

2.7.3. Immuno-histochemistry

Paraffin sections prepared as described above were deparaffinized in xylene and rehydrated in a descending ethanol series, including a blocking step using 10% hydrogen peroxidase for 20 min to block endogenous peroxidase. The antigens were retrieved by incubating the sections in 1% trypsin in PBS for 15 min. Pre-incubation with 10% normal goat serum (Jackson ImmunoResearch, Inc. West Grove, PA, USA) in PBS for 10 min to suppress non-specific staining was followed by incubation with primary antibody mouse anti-rat osteocalcin (OC4-30, 1:400; Novus Bilogicals, Cambridge, United Kingdom) overnight at 4 °C. Then, the sections were incubated with biotinylated secondary antibody donkey anti-mouse IgG (1:500; Jackson ImmunoResearch, Inc.) for 60 min at room temperature prior to subsequent incubations in Biotin-(Strept) Avidin (ABC) complex solution for 45 min and 3,3′diaminobenzidine (DAB) chromogen solution for approximately 10 min. Optical microscope images were acquired with a Zeiss Z1 microscope (Axio Imager Microscope Z1, Carl Zeiss Micro imaging GmbH, Göttingen, Germany).

2.8. Statistical Analysis

The fold-swelling ratio and calcium content measurements were statistically evaluated with GraphPad Instat version 3.06 (GraphPad Software, San Diego CA, USA), using a one-way ANOVA combined with a post-hoc Tukey–Kramer Multiple Comparisons Test to detect statistically significant differences at a significance level (p-value) of $p < 0.05$. Results are presented as means ± stan-standard deviations.

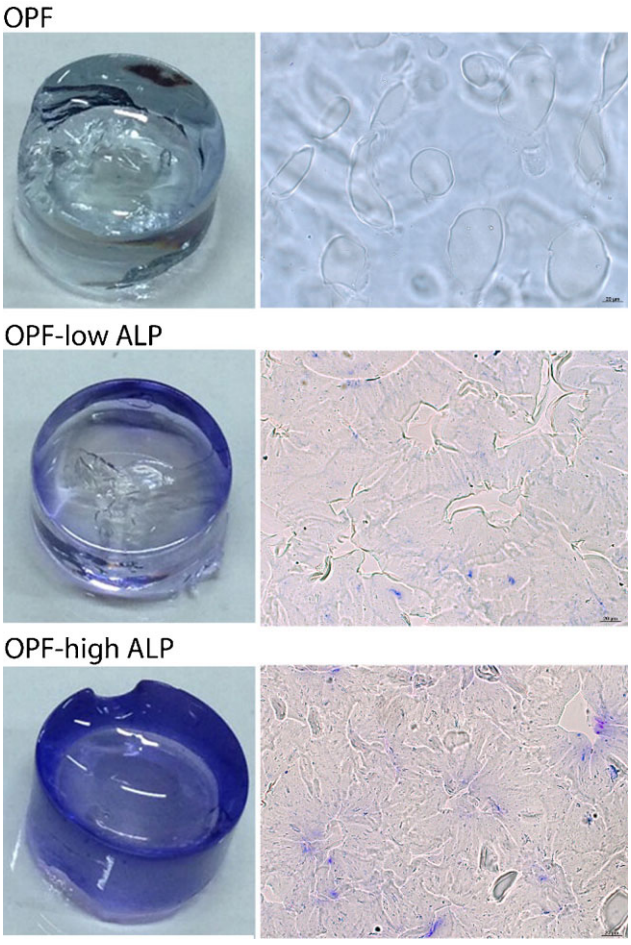

Figure 1. Whole hydrogels and cryosections (50 μm thick) stained with Coomassie brilliant blue. OPF (i.e., ALP-free hydrogels) remained transparent. Blue coloring in ALP-containing OPF increased with increasing enzyme concentration. High magnifications show a plain polymeric matrix for OPF and a uniform distribution of tiny blue dots, as indication of homogenous distribution of the enzyme, in ALP-containing OPF hydrogels (scale bars = 20 μm).

3. Results

3.1. Analysis of ALP Distribution and Diffusion in Hydrogels

Macroscopic and light microscopy images of all of the hydrogels subjected to Coomassie brilliant blue staining are shown in Figure 1. In ALP-enriched OPF hydrogels, ALP (blue color) was homogeneously distributed throughout the scaffolds and the staining intensity increased at higher enzyme concentration. Differently, OPF hydrogels (ALP free) stained negative for ALP.

The diffusion analysis revealed that the fluorescently labeled-dextran diffused equally throughout all hydrogels, regardless of the concentration of ALP present (Figure 2).

3.2. In Vitro Experiments

3.2.1. Hydrogel Swelling Experiment

The swelling ratio of OPF-based hydrogels is shown in Figure 3. The swelling study indicated that equilibrium swelling of the hydrogels was reached after overnight immersion in MilliQ H_2O since all experimental groups revealed swelling ratios of about 25–29. After 2 weeks of soaking in Ca–GP significant differences were observed between the groups. Specifically, plain OPF showed a twofold difference in swelling ratio before (28.1 ± 1.1) and after (56.8 ± 1.3) soaking ($p < 0.001$). OPF-low ALP revealed a statistically higher ($p < 0.01$) swelling ratio after soaking (34.7 ± 0.9) compared to the swelling ratio prior to soaking (29.5 ± 0.3), whereas the swelling ratio of OPF-high ALP remained approximately constant before and after soaking (27.5 ± 2.0 and 28.8 ± 0.4; $p > 0.05$). After soaking, the swelling ratio of plain OPF was considerably larger than both ALP-containing OPF hydrogels ($p < 0.001$), while the swelling ratio of OPF-low ALP was significantly higher than OPF-high ALP ($p < 0.001$).

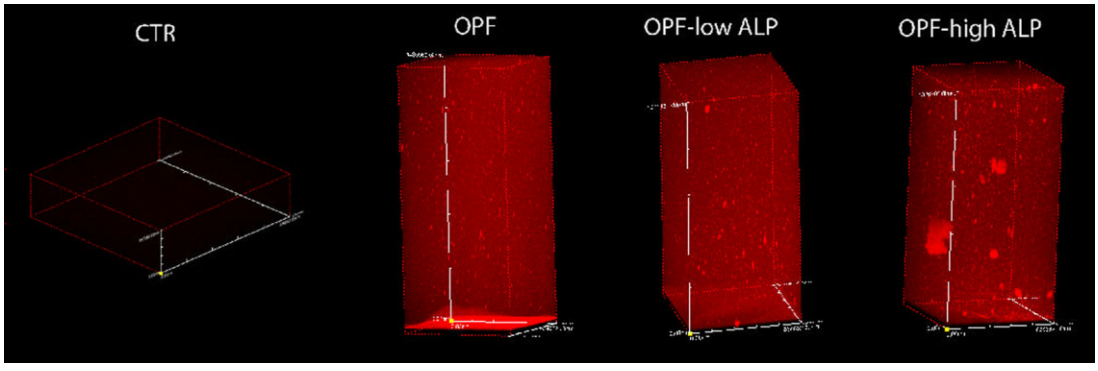

Figure 2. Confocal microscopy of OPF, OPF-low ALP, and OPF-high ALP hydrogels after diffusion (time point: 1 d) of MilliQ H_2O (CTR) and TRITC-dextran solution (red color).

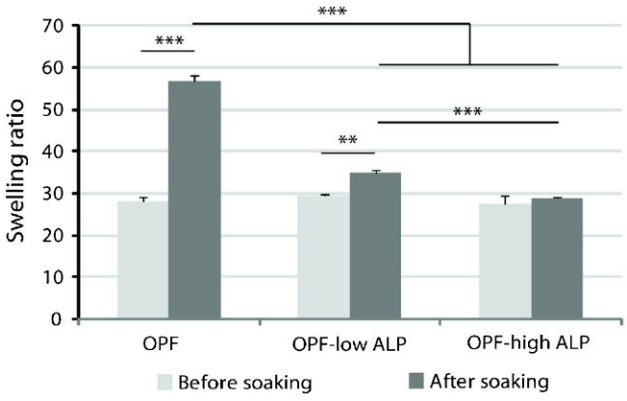

Figure 3. Swelling ratio of OPF, OPF-low ALP, and OPF-high ALP before soaking and after soaking (2 weeks) in 10 mM Ca–GP. $^{**}p < 0.01$ and $^{***}p < 0.001$. Error bars represent means ± standard deviation.

3.2.2. Characterization of Biomineralization: ATR-FTIR, XRD, and Calcium Assay

The macroscopic appearance of hydrogels before and after soaking in 10 mM Ca–GP is depicted in Figure 4A. By the 14th day of incubation in 10 mM Ca–GP, a different appearance between the groups became apparent. Specifically, OPF remained transparent whereas OPF-low ALP became slightly opaque and OPF-high ALP became considerably opaque.

ATR-FTIR spectra of freeze-dried hydrogels are shown in Figure 4B. No apatitic phosphate absorption peaks were detected for any of the hydrogels prior to soaking in Ca–GP. After soaking, OPF spectra remained approximately unchanged (no apatitic phosphate bands). On the contrary, ALP-containing OPF hydrogels displayed spectra in which the characteristic absorption bands of apatitic phosphate (559, 600, 962, and 1 025 cm^{-1}) were clearly detectable.

XRD patterns of mineralized hydrogels are shown in Figure 4C. OPF-high ALP exhibited diffraction peaks at $2\theta = 25.8^{\circ}$ (002) and 31.8° (211) (arrowheads), which

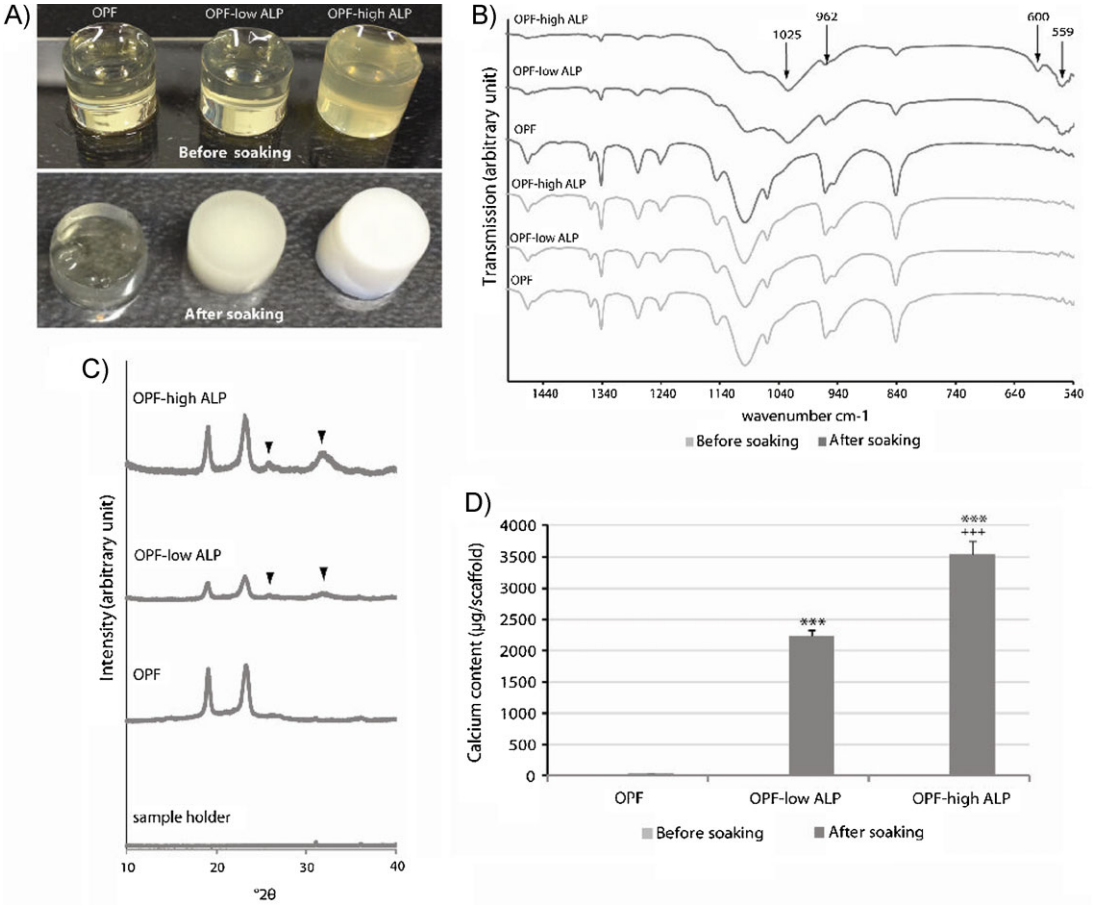

Figure 4. (A) Appearance of OPF, OPF-low ALP, and OPF-high ALP hydrogels before and after 2 weeks of soaking in 10 mM Ca–GP. (B) ATR-FTIR analyses, (C) XRD analyses (arrowheads indicate characteristic peaks of apatite), and (D) calcium content of hydrogels. $^{***}p < 0.001$ relative to OPF; $+++p < 0.001$ relative to OPF-low ALP. Error bars represent means ± standard deviation.

can be attributed to apatite calcium phosphate. These peaks were less pronounced for OPF-low ALP and absent for OPF.

Quantification of the amount of calcium (Figure 4D) revealed the absence of calcium in all hydrogels before soaking. After soaking, OPF showed a negligible amount of calcium ($32.2 \pm 4.0\ \mu g \cdot scaffold^{-1}$). In comparison, a significant increase of calcium content was observed for OPF-low ALP ($2\ 229.8 \pm 96.0\ \mu g \cdot ml^{-1}$; $p < 0.001$) and even more for OPF-high ALP ($3\ 532.8 \pm 226.5\ \mu g \cdot ml^{-1}$; $p < 0.001$). Importantly, the amount of calcium in OPF-high ALP was statistically higher compared to OPF-low ALP ($p < 0.001$).

3.2.3. Structure and Distribution of Minerals: SEM, EDS, and Microscopic Analysis

SEM images of freeze-dried hydrogels are shown in Figure 5. Before soaking, all hydrogels exhibited the typical smooth surface of organic polymers. By the 14th day of soaking, OPF maintained the original polymeric surface. In contrast, ALP-containing OPF hydrogels showed a relatively rough surface (Figure 5A). Specifically, hydrogels were densely mineralized at the hydrogel periphery, whereas the number and size of mineralized structures decreased toward the center of the hydrogels (Figure 5B).

EDS analysis showed a negligible amount of Ca and P in OPF hydrogels, whereas a Ca and P concentration gradient was observed starting from the periphery toward the center of the hydrogels for the ALP-containing hydrogels (Figure 6). Importantly, it was observed that steepness of the concentration gradient increased with increasing ALP concentration.

Microscopical analysis of calcium deposition within cross-sections of the hydrogels is shown in Figure 7. Particularly, high magnification of alizarin red-stained cross-sections of the hydrogel scaffolds showed intensive dark spots (reddish/brown color) along the periphery of the ALP-containing OPF (Figure 7i), and empty areas in the center (Figure 7ii).

3.3. In Vivo Experiment

3.3.1. General Observations

Hydrogel implantation was uneventful for all animals and not accompanied by visible inflammatory reactions (i.e., swelling and redness). All of the scaffolds were retrieved from the subcutaneous tissue of the rats.

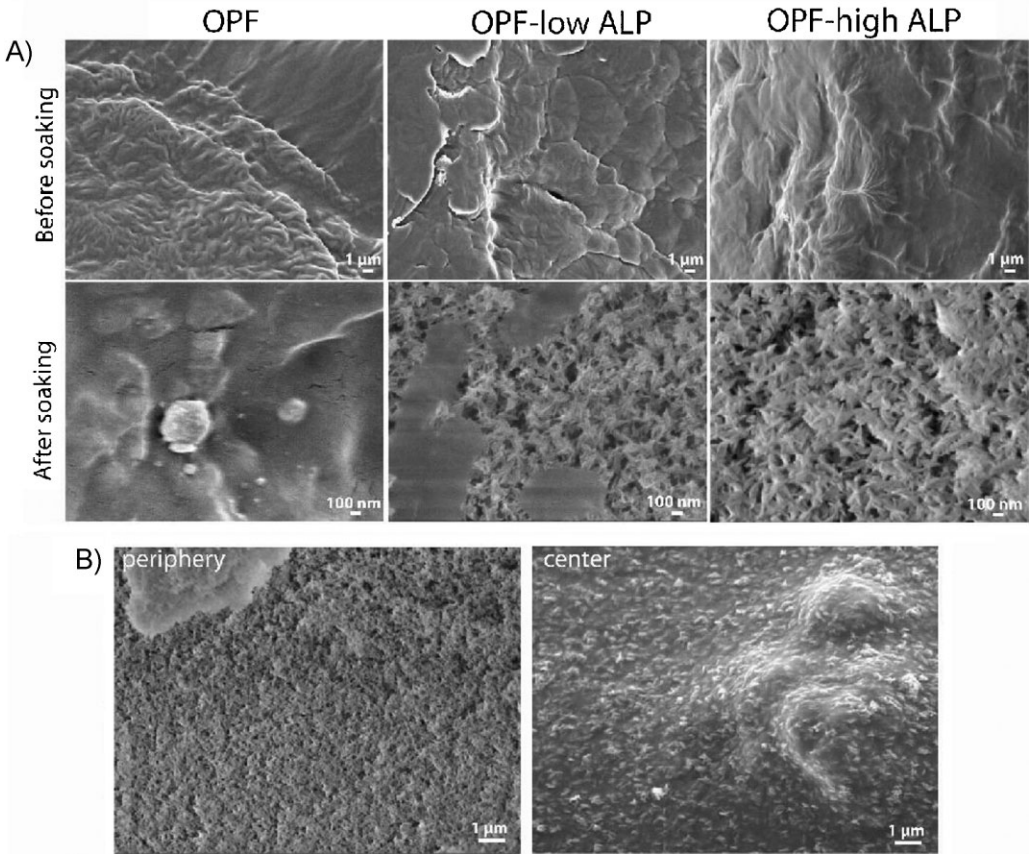

Figure 5. (A) Scanning electron micrographs of freeze-dried hydrogels before and after 2 weeks of soaking in 10 mM Ca–GP. (B) Mineral distribution in the periphery and center of ALP-containing OPF.

Macromol. Biosci. **2013**, DOI: 10.1002/mabi.201200474

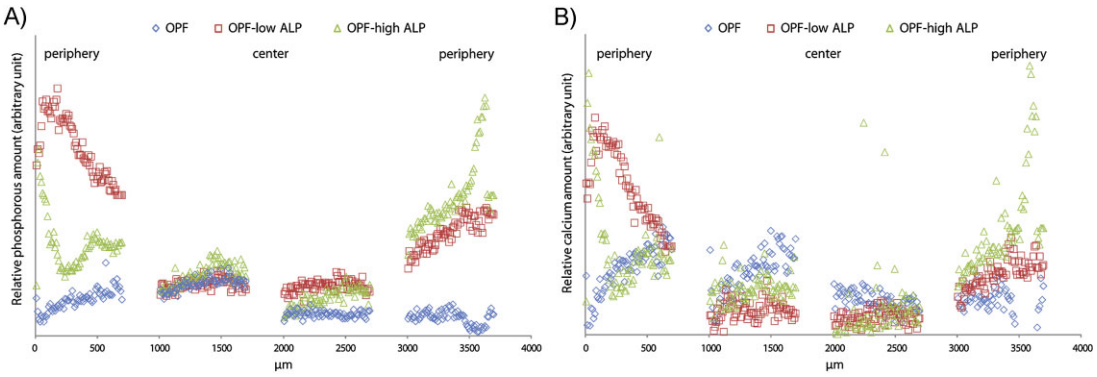

Figure 6. Changes in the relative amount of phosphorous (A) and calcium (B) over a random diagonal of the disc-shaped scaffolds for OPF, OPF-low ALP, and OPF-high ALP after soaking in Ca–GP solution, as determined with EDS analysis.

3.3.2. Histological and Immunological Analysis

Figure 8 presents histological sections of OPF-based hydrogels after a 4-week subcutaneous implantation period. Generally, all hydrogels presented a frayed or damaged structure, with marked cellular infiltration along the periphery (Figure 8A). Nevertheless, the original shape of the hydrogels was clearly recognizable by a thin capsule surrounding the implanted scaffold (yellow dotted line, Figure 8A). Specifically, the soft-tissue capsule (fc) consisted of flattened fibroblasts with oval nuclei and contained blood vessels (arrowheads, Figure 8B). Abundant infiltrating cells (i) were present between the fibrous capsule (fc) and hydrogel remnants (*). Figure 8C and D show alizarin red-stained sections of both OPF and ALP-containing OPF hydrogels at identical locations. OPF did not show the presence of calcium deposits. In contrast, ALP-containing OPF hydrogels presented several calcium-containing structures (red color) with dimensions of ≈5–20 µm in the areas where the cells infiltrated into the scaffolds. Interestingly, these structures were found only on one side of the scaffolds, i.e., close to the epidermis, distributed in a

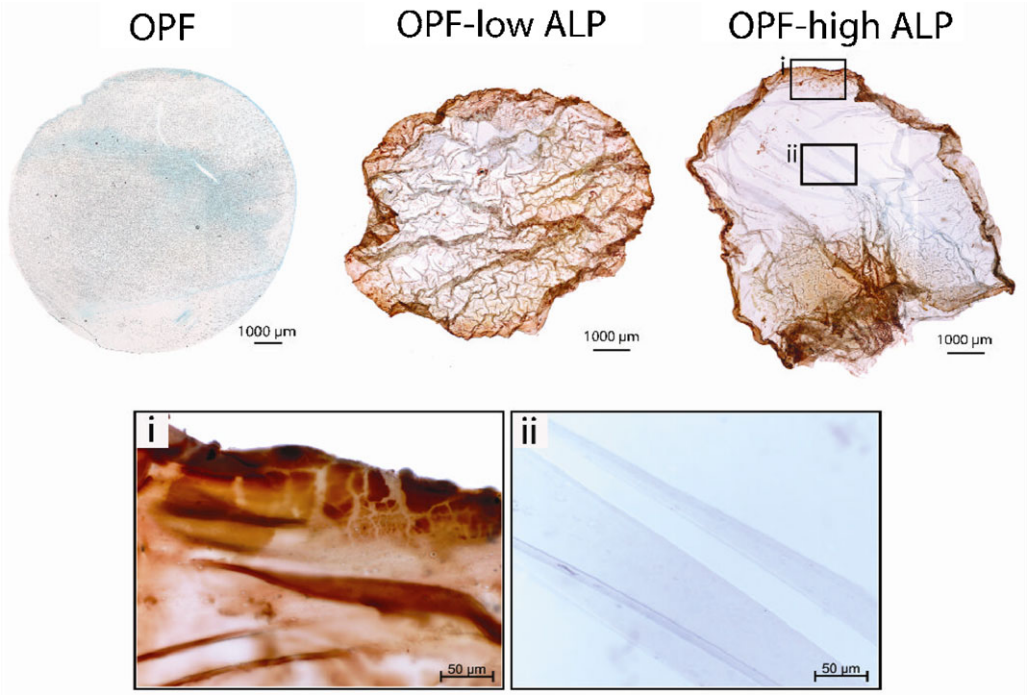

Figure 7. MMA-embedded hydrogels after 2 weeks of soaking in 10 mM Ca–GP and stained with alizarin red to indicate the presence of calcium (scale bars = 1 000 µm). High magnifications of ALP-containing OPF show calcium-enriched and calcium-free areas around the periphery (i) and center (ii) of the hydrogels, respectively (scale bars = 50 µm).

Macromolecular Journals

Macromol. Biosci. **2013**, DOI: 10.1002/mabi.201200474

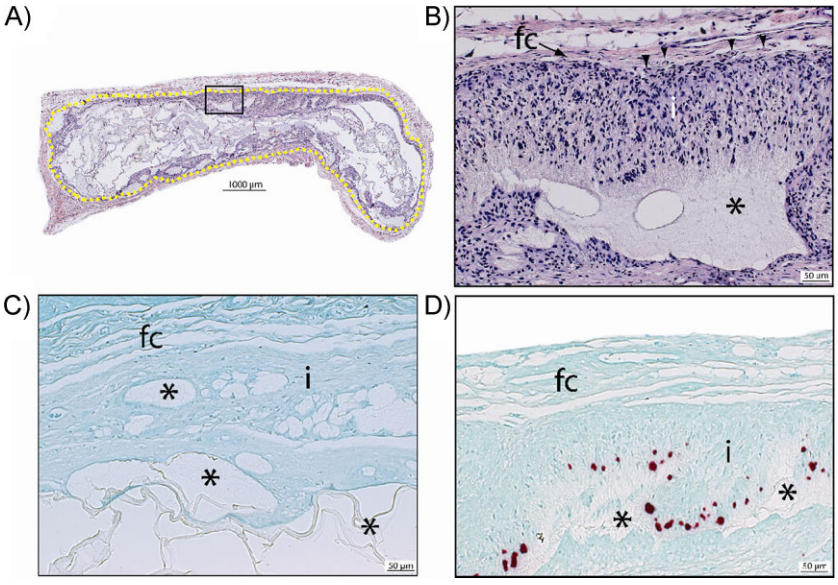

Figure 8. (A) Overview of subcutaneous scaffolds at 4 weeks after implantation stained with hematoxylin and eosin. Yellow dotted line indicates the fc surrounding the hydrogel (scale bar = 1000 μm). (B) Magnification of fc composed of flattened and elongated fibroblasts and blood vessels (arrowheads). Abundant cell infiltration (i) was present between the fc and hydrogel remnants (*) (scale bar = 50 μm). (C) Alizarin red staining shows the absence of calcium in OPF hydrogels (scale bar = 50 μm). (D) Calcium deposits (red dots) were found in ALP-containing hydrogels (scale bar = 50 μm).

wave-like fashion (blue dotted line, Figure 9A). Von Kossa staining confirmed the presence of phosphate-containing deposits (brown color) at the same areas and with a spatial distribution similar to the calcium-containing deposits (Figure 9B). Osteocalcin (i.e., marker for osteoblast differentiation) was not detected in the vicinity of calcium and phosphate deposits (Figure 9C).

4. Discussion

The aim of the present study was to compare the in vitro and in vivo efficacy of ALP to induce biomineralization in OPF hydrogels. To that end, ALP was incorporated into OPF hydrogels at three different concentrations generating three experimental groups (i.e., i) plain OPF, ii) OPF-low ALP (2.5 mg · ml^{-1}), and iii) OPF-high ALP (10 mg · ml^{-1})). The hydrogels were either incubated in a supersaturated solution of Ca-GP (10 mM) for 2 weeks or implanted subcutaneously in the dorsum of rats for 4 weeks. By mimicking the natural mechanism of biomineralization in bone tissue, we hypothesized that: i) ALP would act as a mediator for mineral deposition; and ii) increasing enzyme concentration would increase the hydrolysis rate of the substrate and, therefore, the formation of mineral deposits. The results showed that only ALP-containing hydrogels were able to mineralize in vitro, and that the degree of biomineralization correlated to the enzyme concentration as indicated by the increased opacity and 1.5-fold higher calcium content of OPF-high ALP compared to OPF-low ALP. Nevertheless, the distribution of minerals in both types of ALP-containing OPF hydrogels was inhomogeneous as evidenced by a decreasing concentration gradient of calcium and phosphorus from the periphery to the center of the hydrogels. A similar – albeit less pronounced – biomineralization capacity was observed at the periphery of ALP-containing OPF hydrogels after four-week subcutaneous implantation. This mineralizing capacity did not depend on the ALP concentration.

Simulated body fluid (SBF), a solution with ion concentrations and a pH value similar to that of human blood plasma,[29] is extensively used in research to induce mineralization of hydrogel composites.[9,11,30] In addition, supersaturated calcium and glycerophosphate solutions provide an alternative and more practical method of inducing formation of minerals as it requires a short-term exposure to substrates. Previously, ALP was used to direct enzymatic mineralization of hydrogels by soaking in a supra-physiological concentration of exogenous organic phosphate esters in a range of 50–100 mM of Ca–GP.[14–21] In the present study, the choice to use a concentration of 10 mM Ca–GP for the in vitro study was based on the concentration of organic phosphate estimated to be present in the physiological environment.[31] Interestingly, we proved that 10 mM Ca–GP is sufficient to serve as a substrate for ALP to supply inorganic phosphate within OPF hydrogels and promote biomineralization in vitro.

The homogeneous distribution of ALP throughout the hydrogels, as shown by Coomassie brilliant blue staining, could not compromise the diffusion of β-glycerophosphate (MW 210.14) in ALP-containing OPF hydrogels as it did not thwart the diffusion of a larger compound, such as dextran (molecular weight (MW) = 10 000 Da). However, the diffusion of the substrate (i.e., Ca–GP) together with a rather high activity of the ALP most likely resulted into a rapid saturation of free PO_4^{3-} ions at the periphery of the ALP-containing hydrogels that subsequently precipitated as apatitic CaP deposits. This precipitation at the hydrogel periphery formed a mineralized shell that further decelerated substrate diffusion into the center of the hydrogels and created a gradient distribution of minerals as confirmed by SEM, EDS, and microscopical observation. These results are consistent with previous findings[14] and explain why the

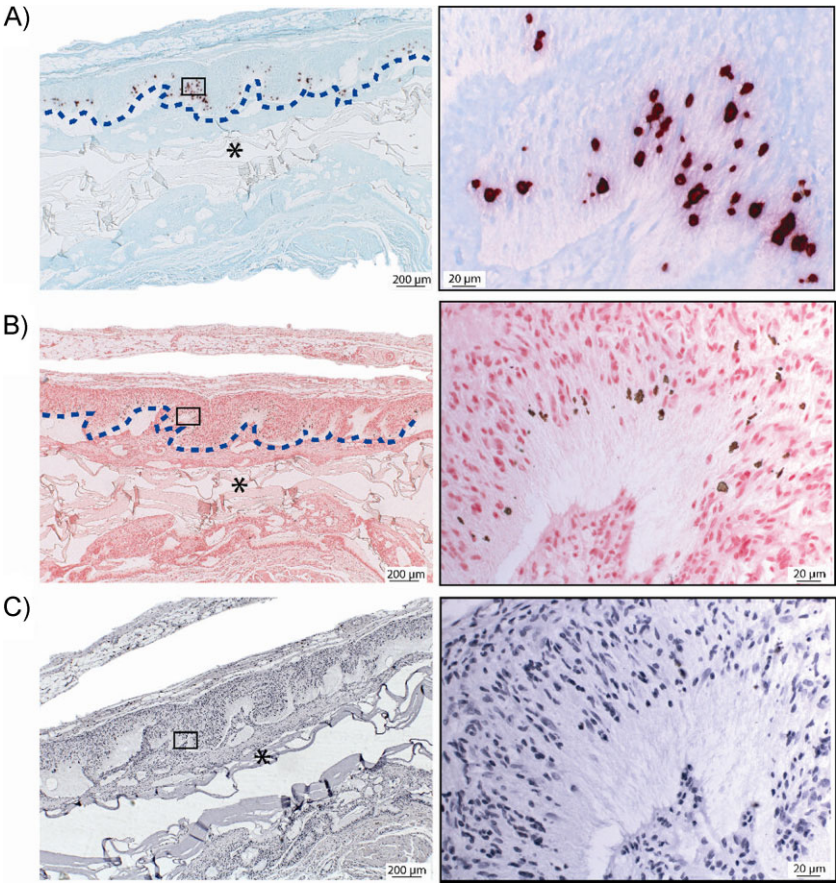

Figure 9. (A) Alizarin red (B) Von Kossa, and (C) osteocalcin-stained sections of OPF-ALP hydrogels. The blue dotted-lines follow the wave-like deposition of calcium-containing (A, red dots) and phosphate-containing (B, brown dots) deposits (scale bars = 20 μm) (* indicates hydrogel). The panels on the right show magnifications of the boxes indicated in the panels on the left (scale bars = 20 μm). Osteocalcin positive staining was not observed in the areas of positive calcium and phosphate staining.

calcium level in OPF-high ALP hydrogels increased only 1.5-fold compared to OPF-low ALP even though the ALP concentration was fourfold higher. Of note, in the aforementioned study,[14] as in ours, the relatively large width (≈1.0 cm) and thickness (≈1.5 cm) of the hydrogels accentuated the "mineralized shell phenomenon" compared to small-size hydrogels (e.g., beads), in which the shorter path for substrate (calcium and β-glycerophosphate) diffusion led to a greater homogeneity of mineral deposition.[21]

For OPF, the degradation via hydrolysis of ester bonds[25] was responsible for the increase in the swelling after soaking in Ca–GP. Specifically, the hydrolysis resulted in a decrease of the crosslinking density as well as of the final polymer dry weight, thereby enhancing the swelling ratio. For ALP-enriched OPF, two processes (i.e., degradation of OPF and mineral formation) occurred simultaneously. The polymer degradation would increase the swelling ratio, whereas mineral formation would increase the dry weight and decrease the swelling ratio. According to the results presented in Figure 3, the added mass due to mineral formation was large enough to compensate for the results of polymer degradation such that the net change in swelling ratio was small for OPF-low ALP hydrogels and almost zero for OPF-high ALP hydrogels. Of note, the formation of minerals results in an enhancement of mechanical properties of the hydrogels containing ALP, as previously demonstrated by Douglas et al.[14]

While several studies have heretofore focused on ALP-mediated enzymatic mineralization of hydrogels in vitro, the current study is the first attempt to evaluate the enzymatic mineralization capacity of synthetic hydrogels in vivo. Similar to the in vitro study, only ALP-containing OPF hydrogels showed biomineralization ability. Specifically, mineral deposits were formed at the periphery near the tissue/hydrogel interface. These mineral deposits did not originate from osteoblast differentiation and mineralization, as osteocalcin was absent in the mineralized areas. Most likely, the highly vascularized dermis and the abundant infiltrating cells present in the periphery of the hydrogels were the principal source of organic phosphate, which became available for ALP to promote mineralization.[13] Nonetheless, the discrepancy between the in vitro and in vivo effect of ALP (i.e., strong mineralization vs. weak mineralization) on hydrogel biomineralization remains to be elucidated. Previous reports have demonstrated that the optimal activity of ALP in vitro is affected by a combination of parameters, including substrate concentration, temperature, and pH (between 7 and 10).[32,33] However, while all these parameters can be precisely controlled and adjusted in vitro, the extreme complexity of the physiological environment (including proteins, cells, pH decreasing as a result of the inflammatory response upon tissue damage and scaffold implantation) gives rise to poor predictability in vivo. Here, ALP-mediated mineralization of OPF hydrogels was evaluated in vitro by immersion in 10 mM Ca–GP solution. Yet, it has been argued whether these organic phosphates are hydrolyzable under physiological conditions.[34] Additionally, the phosphate concentration in the blood serum and plasma seem to be much lower than 10 mM (i.e., 1.0–1.5 mM as inorganic phosphate and 3.0 mM as organic phosphate).[35] As reported above, the optimal pH for highest activity of ALP can vary between 7 and 10

depending on other parameters, such as concentration of the substrate and temperature. The pH of the 10 mM Ca–GP solution used in the current study was ≈9.5 and experiments performed at pH 7.4 rendered qualitatively similar results (data not shown). Nevertheless, ALP may not be optimally active at the physiological conditions in vivo. Further analyses will be necessary to study the combination of various parameters in order to better envision the enzymatic activity at a physiological condition. Lastly, the different volume between the two conditions, i.e., 4 ml of 10 mM Ca–GP solution in a 12-well plate in vitro versus an entire animal (≈250 ml volume) in vivo, further explains the lower effect in vivo.

The efficacy of ALP regarding biomineralization is not yet fully understood, as this enzyme is abundantly present in both mineralized and non-mineralized tissues where cells secrete organic phosphates, such as glucose phosphates, glycerophosphates, and adenosine phosphates.[36] In addition to the leading theory on the role of ALP in catalyzing the hydrolysis of phosphate monoester, Robison introduced a "second mechanism" supporting the deposition of minerals in a calcium phosphate supersaturated environment, which is characteristic for mineralized tissues.[37] Furthermore, it appears that ALP plays a role in biological mineralization only when a calcium salt and organic phosphate are released at a rate matching to the rate of alkaline phosphate release.[20] In the current study, hydrogels were implanted in a non-mineralized tissue, where the concentration of calcium and organic phosphate and the free phosphate ions released by ALP could be too low to initiate mineral deposition. This explanation is likely in view of the minor effect of ALP present within OPF hydrogels on biomineralization in vivo compared to in vitro, as shown in the current study.

5. Conclusion

The in vitro and in vivo enzyme-mediated biomineralization capacity of OPF hydrogels was evaluated by incubating hydrogels in a β-glycerophosphate-containing solution and subcutaneous implantation in rats, respectively. The in vitro results showed that OPF hydrogels exhibited a strong ability to mineralize upon incorporation of ALP, which increased with increasing ALP concentration. Nevertheless, mineral deposition was not homogeneous throughout the hydrogels, but restricted to their periphery. Similar to the in vitro data, only ALP-containing hydrogels induced mineralization in vivo. Specifically, small (≈5–20 μm) mineral deposits were found at the periphery of the hydrogels near the dermis/scaffold interface, most likely as a result of a higher concentration of organic phosphate from the highly vascularized tissue. Since the role of ALP in mineralization seems to be limited only on calcifying tissues, it will be of considerable importance to investigate the biomineralization ability of injectable ALP-containing OPF hydrogels in an orthotopic bone regeneration model.

Received: December 21, 2012; Revised: February 26, 2013; Published online: DOI: 10.1002/mabi.201200474

Keywords: alkaline phosphatase; biomineralization; bone substitutes; hydrogels; in vivo

[1] L. V. Avioli, S. M. Krane, *Metabolic Bone Disease and Clinically Related Disorders*, 3rd edition, Academic Press, San Diego, California **1998**, p. 314.
[2] S. Weiner, H. D. Wagner, *Annu. Rev. Mater. Sci.* **1998**, *28*, 271.
[3] M. Bongio, J. J. van den Beucken, S. C. G. Leeuwenburgh, J. A. Jansen, *J. Tissue Eng. Regen. Med.* **2012**, DOI: 10.1002/term.1637.
[4] J. L. Drury, D. J. Mooney, *Biomaterials* **2003**, *24*, 4337.
[5] J. F. Mano, R. A. Sousa, L. F. Boesel, N. M. Neves, R. L. Reis, *Compos. Sci. Technol.* **2004**, *64*, 789.
[6] K. Gkioni, S. C. G. Leeuwenburgh, T. E. L. Douglas, A. G. Mikos, J. A. Jansen, *Tissue Eng., Part B: Rev.* **2010**, *16*, 577.
[7] M. Bongio, J. J. J. P. van den Beucken, M. R. Nejadnik, S. C. G. Leeuwenburgh, L. A. Kinard, F. K. Kasper, A. G. Mikos, J. A. Jansen, *Eur. Cell. Mater.* **2011**, *22*, 359.
[8] S. C. G. Leeuwenburgh, J. A. Jansen, A. G. Mikos, *J. Biomater. Sci. Polym. Ed.* **2007**, *18*, 1547.
[9] M. R. Nejadnik, A. G. Mikos, J. A. Jansen, S. C. G. Leeuwenburgh, *J. Biomed. Mater. Res. A* **2012**, *100*, 1316.
[10] S. Sowmya, P. T. Sudheesh Kumar, K. P. Chennazhi, S. V. Nair, H. Tamura, R. Jayakumar, *Trends Biomater. Artif. Organs* **2011**, *25*, 1.
[11] M. Azami, M. J. Moosavifar, N. Baheiraei, F. Moztarzadeh, J. Ai, *J. Biomed. Mater. Res. A* **2012**, *100*, 1347.
[12] K. Furuichi, Y. Oaki, H. Ichimiya, J. Komotori, H. Imai, *Sci. Technol. Adv. Mater.* **2006**, *7*, 219.
[13] W. Beertsen, T. van den Bos, *J. Clin. Invest.* **1992**, *89*, 1974.
[14] T. E. Douglas, P. B. Messersmith, S. Chasan, A. G. Mikos, E. L. W. de Mulder, G. Dickson, D. Schaubroeck, L. Balcaen, F. Vanhaecke, P. Dubruel, J. A. Jansen, S. C. G. Leeuwenburgh, *Macromol. Biosci.* **2012**, *12*, 1077.
[15] G. Liu, D. C. Zhao, A. P. Tomsia, A. M. Minor, X. Y. Song, E. Saiz, *J. Am. Chem. Soc.* **2009**, *131*, 9937.
[16] J. Li, H. Wu, Y. Liang, Z. Jiang, Y. Jiang, L. Zhang, *J. Biomater. Sci., Polym. Ed.* **2013**, *24*, 199.
[17] J. Song, E. Saiz, C. R. Bertozzi, *J. Am. Chem. Soc.* **2003**, *125*, 1236.
[18] E. Golub, K. Boesze-Battaglia, *Curr. Opin. Orthop.* **2007**, *18*, 444.
[19] R. Robison, *Biochem. J.* **1923**, *17*, 286.
[20] E. Banks, S. Nakajima, I. C. Shapiro, O. Tilevitz, J. R. Alonzo, R. R. Chianelli, *Science* **1977**, *198*, 4322.
[21] M. L. Xie, M. O. Olderoy, Z. B. Zhang, J. P. Andreassen, B. L. Strand, P. Sikorski, *RSC Adv.* **2012**, *2*, 1457.
[22] E. D. Spoerke, S. G. Anthony, S. I. Stupp, *Adv. Mater.* **2009**, *21*, 425.
[23] S. P. Bruder, A. I. Caplan, *Bone* **1990**, *11*, 133.
[24] J. S. Temenoff, H. Park, E. Jabbari, T. L. Sheffield, R. G. LeBaron, C. G. Ambrose, A. G. Mikos, *J. Biomed. Mater. Res., A* **2004**, *70*, 235.

[25] H. Shin, P. Quinten Ruhé, A. G. Mikos, J. A. Jansen, *Biomaterials* **2003**, *24*, 3201.
[26] M. Bongio, J. J. van den Beucken, M. R. Nejadnik, Z. T. Birgani, P. Habibovic, L. A. Kinard, F. K. Kasper, A. G. Mikos, S. C. Leeuwenburgh, J. A. Jansen, *Acta Biomater.* **2013**, *9*, 5464.
[27] L. A. Kinard, F. K. Kasper, A. G. Mikos, *Nat. Protoc.* **2012**, *7*, 1219.
[28] H. Park, X. Guo, J. S. Temenoff, Y. Tabata, A. I. Caplan, F. K. Kasper, A. G. Mikos, *Biomacromolecules* **2009**, *10*, 541.
[29] T. Kokubo, H. Kushitani, S. Sakka, T. Kitsugi, T. Yamamuro, *J. Biomed. Mater. Res.* **1990**, *24*, 721.
[30] X. Liu, L. A. Smith, J. Hu, P. X. Ma, *Biomaterials* **2009**, *30*, 2252.
[31] H. C. Tenenbaum, J. N. Heersche, *Calcif. Tissue Int.* **1982**, *34*, 76.
[32] C. Hoffmann, C. Zollfrank, G. Ziegler, *J. Mater. Sci.: Mater. Med.* **2008**, *19*, 907.
[33] M. H. Ross, J. O. Ely, J. G. Archer, *J. Biol. Chem.* **1951**, *192*, 561.
[34] H. I. Khouja, A. Bevington, G. J. Kemp, R. G. G. Russell, *Bone* **1990**, *11*, 385.
[35] C. H. Chung, E. E. Golub, E. Forbes, T. Tokuoka, I. M. Shapiro, *Calcif. Tissue Int.* **1992**, *51*, 305.
[36] E. Henrichsen, *Exp. Cell Res.* **1956**, *11*, 511.
[37] R. Robison, M. Macleod, A. H. Rosenheim, *Biochem. J.* **1930**, *24*, 1927.

Macromol. Biosci. **2013**, DOI: 10.1002/mabi.201200474